International Journal of Pharmaceutics 651 (2024) 123763

Contents lists available at ScienceDirect

International Journal of Pharmaceutics

journal homepage: www.elsevier.com/locate/ijpharm

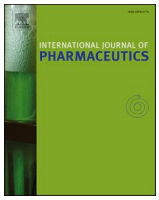

Hyaluronic acid-functionalized graphene-based nanohybrids for targeted breast cancer chemo-photothermal therapy

Rita Lima-Sousa [a], Bruna L. Melo [a], António G. Mendonça [a,b], Ilídio J. Correia [a,c,*], Duarte de Melo-Diogo [a,*]

[a] CICS-UBI – Centro de Investigação em Ciências da Saúde, Universidade da Beira Interior, 6200-506 Covilhã, Portugal
[b] Departamento de Química, Universidade da Beira Interior, 6201-001 Covilhã, Portugal
[c] CIEPQPF – Departamento de Engenharia Química, Universidade de Coimbra, 3030-790 Coimbra, Portugal

ARTICLE INFO

Keywords:
Cancer
Chemo-Photothermal therapy
Hyaluronic acid
Reduced Graphene Oxide
Targeted therapy

ABSTRACT

Nanomaterials' application in cancer therapy has been driven by their ability to encapsulate chemotherapeutic drugs as well as to reach the tumor site. Nevertheless, nanomedicines' translation has been limited due to their lack of specificity towards cancer cells. Although the nanomaterials' surface can be coated with targeting ligands, such has been mostly achieved through non-covalent functionalization strategies that are prone to premature detachment. Notwithstanding, cancer cells often establish resistance mechanisms that impair the effect of the loaded drugs. This bottleneck may be addressed by using near-infrared (NIR)-light responsive nanomaterials. The NIR-light triggered hyperthermic effect generated by these nanomaterials can cause irreversible damage to cancer cells or sensitize them to chemotherapeutics' action. Herein, a novel covalently functionalized targeted NIR-absorbing nanomaterial for cancer chemo-photothermal therapy was developed. For such, dopamine-reduced graphene oxide nanomaterials were covalently bonded with hyaluronic acid, and then loaded with doxorubicin (DOX/HA-DOPA-rGO). The produced nanomaterials showed suitable physicochemical properties, high encapsulation efficiency, and photothermal capacity. The *in vitro* studies revealed that the nanomaterials are cytocompatible and that display an improved uptake by the CD44-overexpressing breast cancer cells. Importantly, the combination of DOX/HA-DOPA-rGO with NIR light reduced breast cancer cells' viability to just 23 %, showcasing their potential chemo-photothermal therapy.

1. Introduction

Small molecule driven approaches have been the main resource for treating cancer (Zhong et al., 2021). Despite the intense research, the currently available chemotherapeutic molecules are still plagued by poor efficacy and weak selectivity towards cancer cells (Ankathil, 2019; Gyanani et al., 2021). This last issue is responsible for the known side effects induced by chemotherapy, that can span from nausea and hair loss to severe organ complications (*e.g.*, liver disfunction, cardiovascular problems) (Kuderer et al., 2022).

Over the years, different types of technological approaches have been explored to address these limitations of the chemotherapeutic drugs (Wei et al., 2021). In particular, the use of nanomaterials for cancer therapy has been providing exciting results (Cheng et al., 2021). Nanoparticles can encapsulate chemotherapeutic drugs in their core/reservoirs, hence increasing the drugs' solubility (Cheng et al., 2021; Dutta et al., 2021). One of the most notable characteristics of the nanoparticles is their capacity to passively accumulate within the tumor site, through the so-called enhanced permeability and retention effect (Alves et al., 2022b; Attia et al., 2019). In this way, drug-loaded

Abbreviations: ANOVA, Analysis of Variance; CLSM, Confocal Laser Scanning Microscopy; Cys, Cysteine; DLS, Dynamic Light Scattering; DMEM-F12, Dulbecco's Modified Eagle Medium F12; DOPA-rGO, Dopamine-reduced Graphene Oxide; DOX, Doxorubicin; DOX/HA-DOPA-rGO, DOX loaded HA-functionalized DOPA-rGO; EDC, 1-Ethyl-3-(3-dimethylaminopropyl) carbodiimide; FBS, Fetal Bovine Serum; FTIR, Fourier Transform Infrared; GO, Graphene Oxide; HA, Hyaluronic Acid; HA-SH, Cysteine-grafted HA; MCF-7, Michigan Cancer Foundation-7; NHDF, Normal Human Dermal Fibroblasts; NHS, *N*-Hydroxysuccinimide; NIR, Near Infrared; PBS, Phosphate Buffered Saline; PFA, Paraformaldehyde; PI, Propidium Iodide; TEM, Transmission Electron Microscopy; Tris, tris(hydroxymethyl)aminomethane; RB, Rhodamine B; S.D., Standard Deviation.

* Corresponding authors at: CICS-UBI – Centro de Investigação em Ciências da Saúde, Universidade da Beira Interior, 6200-506 Covilhã, Portugal.
E-mail addresses: icorreia@ubi.pt (I.J. Correia), demelodiogo@fcsaude.ubi.pt (D. de Melo-Diogo).

https://doi.org/10.1016/j.ijpharm.2023.123763
Received 12 October 2023; Received in revised form 28 December 2023; Accepted 30 December 2023
Available online 2 January 2024

nanomaterials have the potential to deliver high drug-dosages at the tumor site, with lower systemic exposure (Yan et al., 2020a; Yao et al., 2020). Such is crucial to improve the efficacy and safety of the chemotherapeutic agents.

Despite all these exciting results, the harsh reality is that the clinical translation of nanomedicines has been slow (Hua et al., 2018). This fact can be attributed to a multitude of complex factors, namely to the inability of most nanomedicines to be specifically internalized by cancer cells and to the drug resistance mechanisms developed by cancer cells (Bukowski et al., 2020; Cheng et al., 2021; Liu et al., 2023; Mitchell et al., 2021; Ortíz et al., 2021). The first challenge (lack of selectivity) can be addressed by functionalizing nanomaterials with targeting ligands (Clemons et al., 2018; Pearce and O'Reilly, 2019). Cancer cells overexpress several receptors on their membrane (*e.g.,* folate receptor, transferrin receptor, CD44 receptor) and, thus, nanoparticles can be functionalized with the respective ligands (*e.g.*, folic acid, transferrin, hyaluronic acid) to improve their selectivity (Clemons et al., 2018; Pearce and O'Reilly, 2019; Tian et al., 2022). The production of targeted nanomaterials is often achieved by non-covalently coating the nanomaterials with amphiphilic polymers containing the targeting agent (*e.g.*, DSPE-PEG-FA) (Cintra et al., 2022; Granja et al., 2022; Li et al., 2023a; Zhang et al., 2022b). However, this widely used strategy has drawbacks related to the stability of the non-covalent coating (*i.e.,* detachment) and it is also very sensitive to the formulation conditions (*i.e.,* it has a complex scale-up) (Schubert and Chanana, 2018; Shi et al., 2021; Yan et al., 2020b).

Regarding the drug resistance problems, nanomaterials can also be engineered to exert their therapeutic effect by alternative pathways. In particular, some types of nanomaterials can induce hyperthermic effects upon interaction with light (Chien et al., 2019; Huang et al., 2023; Sun et al., 2024; Zhang et al., 2022a). In this therapeutic approach, raising the temperature to 50 °C (or higher) can provoke irreversible harmful effects on cancer cells (*e.g.*, protein denaturation, cell membrane collapse, enzymatic dysfunction). Cumulatively, these effects can induce the death of cancer cells through necrosis (Chu and Dupuy, 2014). In cancer photothermal applications, it is also fundamental to use near-infrared (NIR; 750 – 1000 nm) light due to its high penetration depth and minimal interactions with endogenous molecules (*e.g.*, water, melanin, proteins) (Alves et al., 2022b). In this way, NIR-light absorbing nanomaterials hold the potential to exert a spatio-temporal controlled effect that is weakly-prone to be affected by the resistance mechanisms established by cancer cells (Alves et al., 2022b). Still, nanomaterials mediated photothermal therapy can prompt a non-homogeneous heat distribution within the tumor (Jiang et al., 2021; Ren et al., 2022). Such results from the nanoparticles higher accumulation in the outer/external areas of the tumor mass, rendering the deep-seated cancer cells unexposed to the photothermal effect (Jiang et al., 2021).

This peripheric effect of nanomaterials' photothermal therapy can be addressed by combining it with chemotherapeutic drugs. In brief, chemotherapeutic drugs can be loaded into the NIR-responsive nanomaterials (Khafaji et al., 2019; Patel et al., 2022). Subsequently, when these are exposed to NIR light, the attained photothermal heating can: i) induce damage on cancer cells (mostly on tumor's periphery), ii) trigger the release of the loaded drugs (which can then diffuse to deeper tumor zones), and iii) sensitize cancer cells to the action of chemotherapeutics (Khafaji et al., 2019; Patel et al., 2022). This last ability also opens a venue for synergistic chemo-photothermal effects by increasing cancer cells' permeability to the drugs and inhibiting the DNA repair mechanisms (which can impair the chemotherapeutic agents' action) (Li et al., 2019).

In this work, a novel covalently functionalized targeted NIR-absorbing nanomaterial for cancer chemo-photothermal therapy was developed. For such, and for the first time, dopamine-reduced graphene oxide (DOPA-rGO) nanomaterials were covalently bonded with hyaluronic acid (HA), and then loaded with doxorubicin (DOX, a model chemotherapeutic drug). DOPA-rGO was selected due to its high photothermal capacity in response to NIR light, and surface chemistry. The catechol-based surface of DOPA-rGO serves a dual role: i) it is compatible with Michael-type additions, enabling covalent functionalization approaches (Li et al., 2023b), and ii) allows the encapsulation of a wide variety of molecules through non-covalent attachment (hydrophobic-hydrophobic interactions or π-π stacking) (Melo et al., 2023). In turn, HA was chosen because of its capacity to bind to the CD44 receptors, which are overexpressed on the membranes of cancer cells. To bind HA to DOPA-rGO, the former was grafted with cysteine, yielding HA-SH. Then, DOPA-rGO was covalently functionalized with HA-SH, through a Michael-type addition, followed by loading of DOX, and their potential for breast cancer chemo-photothermal therapy was investigated.

2. Materials and methods

2.1. Materials

HA (extra low molecular weight, 8000–15,000 Da) and DOX were acquired from Carbosynth (Berkshire, UK). *N*-Hydroxysuccinimide (NHS), cysteine (Cys), graphene oxide (GO), Dulbecco's modified eagle medium F12 (DMEM-F12), fetal bovine serum (FBS), penicilin/streptomycin, rhodamine B (RB), triton X-100 and paraformaldehyde (PFA) were all bought from Sigma Aldrich (Lisboa, Portugal). 1-Ethyl-3-(3-dimethylaminopropyl) carbodiimide (EDC) and calcein-AM were purchased from Merck Life Science (Algés, Portugal). Dopamine Hydrochloride is from Acros Organics (Geel, Belgium) and tris (hydroxymethyl)aminomethane (Tris) is from Fisher Scientific (Oeiras, Portugal). Michigan cancer foundation-7 (MCF-7) was acquired from ATCC (Middlesex, UK) and normal human dermal fibroblasts (NHDF) from Promocell (Heidelberg, Germany). Hoechst 33342® was obtained from Invitrogen (Massachusetts, USA) and propidium iodide (PI) from Alfa Aesar (Kandel, Germany). T-flasks and cell culture plates were gotten from Thermofisher Scientific (Massachusetts, USA). Plates for cell imaging were bought from Ibidi GmbH (Munich, Germany). The water utilized in all experiments was double deionized (0.22 μm filter, 18.2 MΩ cm), and GO underwent 6 h of sonication prior to its use.

2.2. Methods

2.2.1. Production of DOX loaded HA-functionalized DOPA-rGO

The production of the DOX loaded HA-functionalized DOPA-rGO (DOX/HA-DOPA-rGO) was a tri-step process. First, the DOPA-rGO was produced by reacting an aqueous solution of GO (500 μg/mL; 1 mL; pH 8.5) and dopamine (2500 mg) for 4 h at 60 °C, according to the method established by our team (Lima-Sousa et al., 2021). Afterwards, the DOPA-rGO (500 μg/mL, 1 mL, in 10 mM Tris pH 8.5) was covalently functionalized with HA-SH (1000 μg; the synthesis of HA-SH is described in the Supplementary Information) through a Michael-type addition, under sonication for 1 h. This solution was then dialyzed against water for 2 h (14 kDa molecular weight cut-off membrane), yielding HA-DOPA-rGO. Finally, DOX (118.4 μg in methanol) was added to the HA-DOPA-rGO (200 μg/mL, 1 mL), sonicated for 1 h, and dialyzed against water to remove non-loaded DOX (0.5–1 KDa molecular weight cut-off membrane) for 2 h, yielding DOX/HA-DOPA-rGO.

2.2.2. Characterization of HA-DOPA-rGO and DOX/HA-DOPA-rGO

Fourier transform infrared (FTIR) spectroscopy analysis was conducted to validate the successful coating of DOPA-rGO with HA-SH. The size distribution of DOPA-rGO, HA-DOPA-rGO and DOX/HA-DOPA-rGO was analyzed by Dynamic light scattering (DLS) using a Zetasizer Nano ZS (Malvern Instruments, Worcestershire, UK) at a 173° scattering angle. The same equipment was used to determine the charge of the nanomaterials in biologically mimicking medium (DMEM-F12 supplemented with 10 % (v/v) of FBS). The colloidal stability of HA-DOPA-rGO and DOX/HA-DOPA-rGO was evaluated by recording their size changes

over time when dispersed in biologically mimicking medium by DLS. The size and morphology of HA-DOPA-rGO and DOX/HA-DOPA-rGO were examined through Transmission electron microscopy (TEM). To facilitate the samples' imaging, these underwent staining with phosphotungstic acid (2 % (w/v)) prior to their analysis in an HT7700 Transmission electron microscope (Hitachi Ltd., Tokyo, Japan; operated at an acceleration voltage of 80 kV). The ability of the produced nanomaterials to absorb NIR light was assessed in an Evolution 201 spectrophotometer (Thermofisher Scientific, Massachusetts, USA). The content of DOX in DOX/HA-DOPA-rGO was determined by absorption spectroscopy (Melo et al., 2021). Firstly, the absorbance of the DOX/HA-DOPA-rGO samples in water:methanol 1:1 (v/v) was recorded at 808 nm and 498 nm (the standard curves were also performed in water:methanol 1:1 (v/v)). Then, the concentration of DOPA-rGO in DOX/HA-DOPA-rGO was determined by using a standard curve of DOPA-rGO at 808 nm (HA-SH and DOX don't have absorbance at 808 nm). Afterwards, the determined concentration of DOPA-rGO and a standard curve of DOPA-rGO at 498 nm were used to determine its absorption at this specific wavelength. The determined absorption of DOPA-rGO at 498 nm was subtracted to that of the DOX/HA-DOPA-rGO samples (at 498 nm), yielding the absorption of DOX at 498 nm (HA-SH does not have absorbance at this wavelength). Lastly, the determine absorption of DOX at 498 nm and the standard curve of DOX at 498 nm was used to calculate the content of DOX in the DOX/HA-DOPA-rGO samples (Melo et al., 2021).

2.2.3. Evaluation of the nanomaterials' photothermal capacity and NIR light-enhanced drug release

To assess the nanomaterials' photothermal capacity, HA-DOPA-rGO and DOX/HA-DOPA-rGO (at various concentrations) were subjected to NIR light irradiation (808 nm, 1.7 W/cm^2) for up to 5 min, being the resulting temperature increases recorded using a thermocouple thermometer (Alves et al., 2022a). As control, water was also irradiated with NIR light. The selected laser parameters (808 nm, 1.7 W/cm^2, 5 min) were based on previous works that highlighted their safety (Manivasagan et al., 2018; Nave et al., 2023; Peltek et al., 2023). Furthermore, to evaluate the photothermal stability of HA-DOPA-rGO and DOX/HA-DOPA-rGO, these nanomaterials were submitted to five consecutive cycles of NIR laser irradiations (each cycle: 808 nm, 1.7 W/cm^2, 5 min), being the nanomaterials' photothermal capacity, Vis-NIR absorbance and size distribution analyzed (Melo et al., 2023). The nanomaterials were allowed to cool between each irradiation cycle.

The impact of NIR laser irradiation on the release of DOX from DOX/HA-DOPA-rGO was studied following a previously published protocol (Nave et al., 2023). For such, DOX/HA-DOPA-rGO was dissolved in PBS (at pH 7.4), placed into a dialysis membrane (0.5 – 1 kDa molecular weight cut-off), and it was dialyzed against PBS (at pH 7.4) at 37 °C under constant stirring, for a total of 48 h. At predetermined time points, samples were collected and analyzed by absorption spectroscopy to determine the amount of DOX released. During the release assay, one of the groups was exposed to NIR light irradiation (808 nm, 1.7 W/cm^2, 5 min) at the 4 h mark.

2.2.4. Evaluation of the cytocompatibility of HA-DOPA-rGO

For the *in vitro* studies, all cell lines were maintained in culture flasks with DMEM-F12 medium supplemented with FBS (10 % (v/v)) and penicillin/streptomycin (1 % (v/v)), in an incubator with a controlled humidified atmosphere (37 °C; 5 % CO_2).

The cytocompatibility of HA-DOPA-rGO was assessed on breast cancer (using MCF-7 cells) and healthy (using NHDF) cell models (Nave et al., 2023). For this, 1 x 10^4 cells/well were seeded in 96-well plates. After 24 h of growth, the medium was replaced by fresh culture medium containing HA-DOPA-rGO at various concentrations (5 – 100 μg/mL of [DOPA-rGO]). Subsequently, the cells were allowed to incubate for 24 and 48 h in the presence of the nanomaterials. Following this incubation period, fresh culture medium containing resazurin (10 % (v/v)) was incubated with the cells for 4 h in the dark (37 °C, 5 % CO_2). The cellular viability was determined by measuring the fluorescence of resorufin (λ_{ex} = 560 nm; λ_{em} = 590 nm) using a Spectramax Gemini EM Spectrofluorometer (Molecular Devices LLC, USA). Negative control cells were solely incubated with culture medium, while positive control cells were exposed to 70 % (v/v) ethanol.

2.2.5. Evaluation of HA-DOPA-rGO cellular uptake

The uptake of fluorescently labelled HA-DOPA-rGO was investigated in MCF-7 cells (CD44 overexpressing breast cancer cell line) and NHDF (healthy cell line without CD44 overexpression) (Alves et al., 2019). Prior to this analysis, HA-DOPA-rGO (200 μg/mL; 1 mL) was first labelled with RB (fluorescent dye) by a straightforward sonication method (Zhang et al., 2010), being the non-loaded dye removed by dialysis against water (0.5–1 kDa molecular weight cut-off membrane) – RB/HA-DOPA-rGO. The successful labelling of HA-DOPA-rGO with RB was confirmed by DLS and fluorescence spectroscopy. Confocal laser scanning microscopy (CLSM) was employed to observe the uptake of RB/HA-DOPA-rGO by MCF-7 cells and NHDF. In brief, each cell line was seeded in μ-slide 8-well imaging plates at the density of 1.5 x 10^4 cell/well. After totaling 48 h of growth, the cell culture medium was replaced by fresh one containing RB/HA-DOPA-rGO (at 75 μg/mL of [DOPA-rGO]). For comparison purposes, both cell lines were also pre-treated with free HA (*i.e.,* to saturate the CD44 binding sites) for 4 h before the nanomaterials' incubation (Rodrigues et al., 2021). After 4 h of incubation with the nanomaterials, cells were rinsed with a phosphate buffered saline (PBS) solution, fixed with PFA 4 % (w/v) for 15 min at room temperature, and washed again with PBS. The cells' nucleus was labelled with Hoechst 33342® for 30 min (at room temperature), followed by a washing step with PBS. The fluorescence images were acquired in a Zeiss LSM 710 Confocal Microscope (Oberkochen, Germany) using $\lambda_{ex}/\lambda_{em}$ = 405/410–499 nm (Hoechst 33342®) and $\lambda_{ex}/\lambda_{em}$ = 514/513–703 nm (RB). Non-treated cells were used as control. The uptake of RB/HA-DOPA-rGO by MCF-7 cells and NHDF was quantified by fluorescence spectroscopy (Alves et al., 2022a). For such, both MCF-7 cells and NHDF were seeded as described in 2.2.4. Prior to their incubation with RB/HA-DOPA-rGO, cells were also pre-treated with free HA as described above. After 24 h of growth, cells were incubated with fresh culture medium containing RB/HA-DOPA-rGO (75 μg/mL of [DOPA-rGO]) for 4 h. Then, the cells underwent two rounds of rinsing with ice-cold Krebs-Ringer buffer, followed by lysis in Triton X-100 (1 % (v/v) in Krebs-Ringer buffer) under orbital stirring for 30 min. Finally, the fluorescence of RB/HA-DOPA-rGO in the cell lysate was quantified using a spectrofluorometer ($\lambda_{ex}/\lambda_{em}$ = 550/580 nm). Cells only incubated with culture medium were used as the blank.

2.2.6. Evaluation of the photothermal therapy mediated by HA-DOPA-rGO and chemo-photothermal therapy mediated by DOX/HA-DOPA-rGO

The photothermal therapy mediated by HA-DOPA-rGO and chemo-photothermal therapy mediated by DOX/HA-DOPA-rGO were evaluated through the resazurin method (Lima-Sousa et al., 2021). Succinctly, MCF-7 cells were seeded as described in 2.2.4. After 24 h, the cells were incubated with fresh culture medium containing HA-DOPA-rGO (at 50 and 75 μg/mL of [DOPA-rGO]) or DOX/HA-DOPA-rGO (at 27/50 and 40.5/75 μg/mL of [DOX]/[DOPA-rGO]). After 4 h, the cells were irradiated with NIR light (808 nm, 1.7 W/cm^2, 5 min). After 24 h of incubation with these nanomaterials, the cells were incubated with fresh culture medium containing resazurin (10 % (v/v)) for 4 h in the dark (37 °C, 5 % CO_2), being their viability determined as described in section 2.2.4.

For the visualization of the phototherapeutic effects, the MCF-7 cells were seeded in μ-slide 8-well imaging plates as described in the section 2.2.5. After 48 h, the culture medium was replaced with fresh medium containing HA-DOPA-rGO (75 μg/mL of [DOPA-rGO]) or DOX/HA-DOPA-rGO (40.5/75 μg/mL of [DOX]/[DOPA-rGO]) and irradiated with NIR light (808 nm, 1.7 W/cm^2, 5 min) 4 h later. Then, the cells were

stained with calcein-AM and PI for the visualization of live and dead cells, respectively. The fluorescence images were acquired by CLSM using a $\lambda_{ex}/\lambda_{em}$ of 488/493–556 (calcein-AM) and 561/566–719 nm (PI). Cells solely incubated with culture medium were used as control for live cells.

2.2.7. Statistical analysis

The comparison of multiple groups was caried out using the one-way analysis of variance (ANOVA) with the Student–Newman–Keuls test. A *p*-value lower than 0.05 ($p < 0.05$) was considered statistically significant. All data are represented as the mean ± standard deviation (S.D.). The GraphPad Prism v6.0 (Trial version, GraphPad Software, CA, USA) was used for data analysis.

3. Results and discussion

3.1. Production and characterization of HA-DOPA-rGO and DOX/HA-DOPA-rGO

In order to prepare a targeted covalently functionalized nanomaterial for cancer chemo-photothermal therapy, the catechol-based surface of DOPA-rGO (prepared according to the environmentally friendly method previously established by our group (Lima-Sousa et al., 2021)) was covalently conjugated with HA-SH (characterized in the Supplementary Information and in Figure S1) through a Michael-type addition, followed by loading of DOX (DOX/HA-DOPA-rGO) (Fig. 1A).

The successful functionalization of DOPA-rGO with HA-SH was confirmed by FTIR (Figure S2). The DOPA-rGO presented peaks at 1568 cm^{-1} (C = C stretch), 1373 cm^{-1} (C-N stretch) and 1506 cm^{-1} (N–H bend), which are in agreement with the data available in the literature (Huang et al., 2015; Zhang et al., 2018a). The spectrum of HA-SH revelated peaks at 1557 cm^{-1}, 1563 cm^{-1}, and 3289 cm^{-1} corresponding to N–H in secondary amides, N–H bending, and O–H/N–H stretches, respectively (Ashwinkumar et al., 2014). In turn, the HA-DOPA-rGO spectrum displayed the above described characteristics peaks of DOPA-rGO and HA-SH, hence confirming its successful assembly.

Moreover, the DLS analysis confirmed that the functionalization of DOPA-rGO with HA-SH was not detrimental for its size distribution (Fig. 1B). Indeed, both DOPA-rGO and HA-DOPA-rGO exhibited a nanoscale size distribution, falling within the range considered ideal for passive tumor accumulation (Blanco et al., 2015; Etter et al., 2021; Xu et al., 2023a). The TEM analysis further confirmed the lateral dimensions of HA-DOPA-rGO (188 ± 68 nm; Fig. S3C) as well as its sheet-like morphology (Fig. S3A), which is a characteristic of graphene-based nanostructures (Domenech et al., 2020; Melo et al., 2023; Robinson et al., 2011).

The zeta potential analysis revealed that the surface charge of DOPA-rGO was −8.9 ± 0.9 mV, while the HA-DOPA-rGO displayed a surface charge of −10.2 ± 0.8 mV (Figure S4). Considering that HA-based nanomedicines are negatively charged (Kim et al., 2019), this slightly lower surface charge of HA-DOPA-rGO is also indicative of the successful functionalization. As importantly, the surface charge of HA-DOPA-rGO is within the range deemed favorable for cancer-related applications (zeta potential between −10 to + 10 mV) (Blanco et al., 2015).

Then, the chemotherapeutic drug DOX was loaded into the aromatic lattice of HA-DOPA-rGO through hydrophobic interactions and π-π stacking (Alemi et al., 2020; Melo et al., 2023). The DLS analysis confirmed that the loading of DOX into HA-DOPA-rGO did not affect its nanometric size distribution (Fig. 1B). Similarly, the TEM analysis also showed that DOX/HA-DOPA-rGO has a sheet-like morphology and

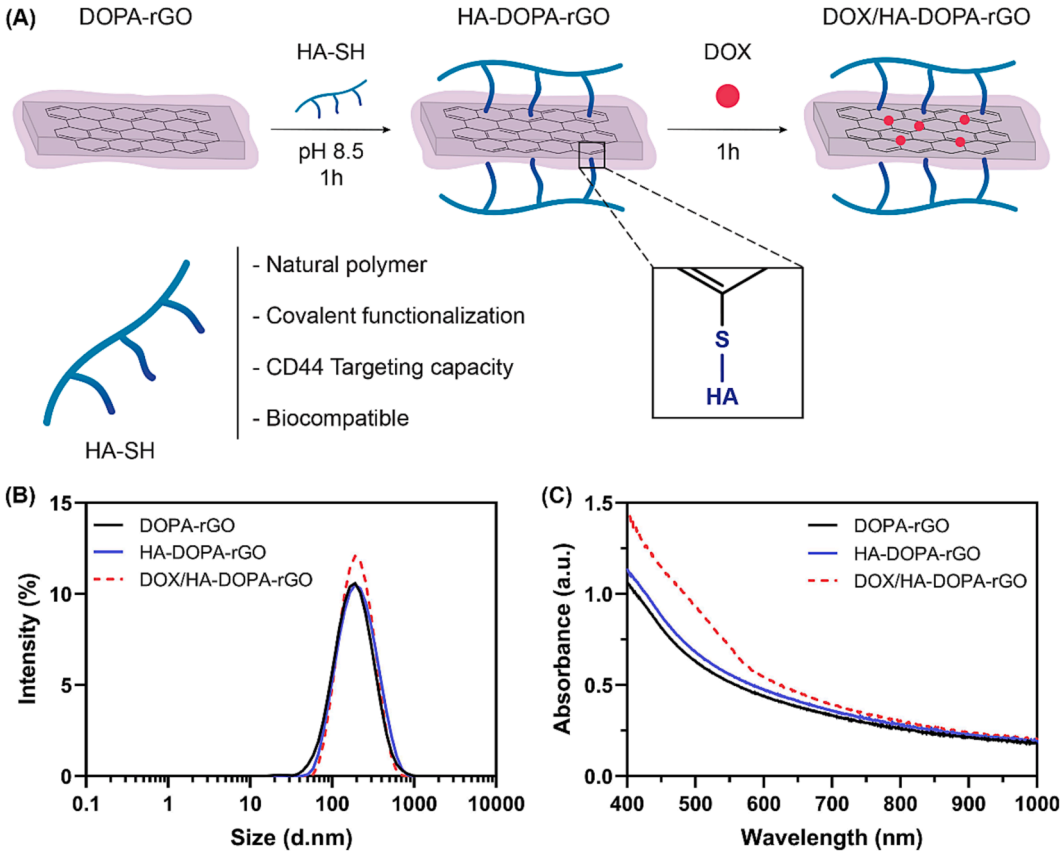

Fig. 1. (A) Schematic representation of the process used to obtain DOX/HA-DOPA-rGO. (B) DLS size distribution of DOPA-rGO, HA-DOPA-rGO and DOX/HA-DOPA-rGO (at 25 μg/mL of [DOPA-rGO]). (C) Visible-NIR absorption spectra of DOPA-rGO, HA-DOPA-rGO and DOX/HA-DOPA-rGO (at 25 μg/mL of [DOPA-rGO]).

nanoscale dimensions (lateral size of 198 ± 77 nm) that resemble those of HA-DOPA-rGO (Fig. S3B and D). The DOX/HA-DOPA-rGO zeta potential was determined to be −7.1 ± 0.3 mV (Figure S4). This increase in the DOX/HA-DOPA-rGO surface charge can be attributed to the loading of DOX, since this molecule has positively charged groups (Hernandes et al., 2023). In fact, the content of DOX in DOX/HA-DOPA-rGO was determined to be 0.541 ± 0.035 μg of DOX per μg of DOPA-rGO, corresponding to a 91.2 % encapsulation efficiency. This ultra-high and ultra-efficient encapsulation can be attributed to the large surface area of HA-DOPA-rGO as well as to its aromatic lattice.

Finally, the stability of HA-DOPA-rGO and DOX/HA-DOPA-rGO in biologically mimicking medium (DMEM-F12 supplemented with 10 % (v/v) of FBS) was evaluated (Fig. S5A). Even after 24 h of incubation in the biologically mimicking medium, the HA-DOPA-rGO and DOX/HA-DOPA-rGO did not suffer any meaningful increase in their dimensions (size variation < 5 %), thus highlighting their excellent colloidal stability.

3.2. Evaluation of the nanomaterials' photothermal capacity and NIR light-enhanced drug release

After corroborating the good physicochemical and optical properties of HA-DOPA-rGO and DOX/HA-DOPA-rGO as well as their excellent colloidal stability, the ability of these nanostructures to interact with NIR light was investigated. In this regard, the HA-DOPA-rGO and DOX/HA-DOPA-rGO displayed a high NIR absorption, being similar to that of DOPA-rGO (Fig. 1C). These findings confirm that the HA-coating and subsequent DOX-loading were not detrimental to the NIR-absorption capacity of this nanomaterial. Subsequently, the heat produced by HA-DOPA-rGO and DOX/HA-DOPA-rGO in response to NIR light (808 nm, 1.7 W/cm^2, 5 min) was assessed (Fig. 2). In this regard, both nanomaterials generated a concentration- and time-dependent temperature increase (ΔT) upon NIR laser irradiation (Fig. 2). At the highest concentration tested (75 μg/mL of [DOPA-rGO]), both HA-DOPA-rGO and DOX/HA-DOPA-rGO generated a photoinduced heat (ΔT) of ≈ 35 °C (Fig. 2A and 2B). Such photothermal effect has the potential to cause significant harm to cancer cells (*e.g.* protein denaturation, cell membrane collapse), ultimately leading to their death by necrosis (Chu and Dupuy, 2014). Furthermore, the temperature increase of water (control) exposed to NIR light was insignificant (ΔT < 4 °C). Such is in agreement with the minimal off-target interaction of NIR light with biological components (Alves et al., 2022b; Lima-Sousa et al., 2021).

For example, Wang and co-workers prepared carboxymethyl cellulose/chitosan nanoparticles that incorporated polypyrrole nanostructures (photothermal agent) and 5-fluorouracil (chemotherapeutic agent) (Wang et al., 2022). When irradiated with NIR light (808 nm, 1.5 W/cm^2, 5 min), these nanohybrid at the concentration of 4000 μg/mL generated a photoinduced heat (ΔT) of 19.8 °C. Lim *et al.* produced CuS nanoparticles containing a mesoporous silica shell that were loaded with DOX and coated with HA (Lim et al., 2020). These nanocomposites at a dose of 250 μg/mL produced a temperature increase of about 15.8 °C in response to NIR light irradiation (808 nm, 2.0 W/cm^2, 5 min). In this work, the HA-DOPA-rGO and DOX/HA-DOPA-rGO at just 75 μg/mL (of [DOPA-rGO]) produced a greater photoinduced heat (ΔT) of ≈ 35 °C (808 nm, 1.7 W/cm^2, 5 min), hence confirming its good photothermal capacity.

Then, the photostability of HA-DOPA-rGO and DOX/HA-DOPA-rGO was assessed by subjecting these nanomaterials to five consecutive NIR laser irradiation cycles (each cycle: 808 nm, 1.7 W/cm^2, 5 min). After five cycles of NIR laser irradiation, these nanomaterials could still generate a photoinduced heat (ΔT) of ≈ 35 °C (Fig. S5B). In this way, the HA-DOPA-rGO and DOX/HA-DOPA-rGO revealed a photostable behavior, being able to elicit an equal temperature variation after one or five consecutive NIR laser exposures (Fig. S5B). The photostability of HA-DOPA-rGO and DOX/HA-DOPA-rGO is likely related to the ability of these nanomaterials to retain their optical absorption after consecutive NIR laser irradiations (Fig. S5C and S5D). The size distribution of HA-DOPA-rGO and DOX/HA-DOPA-rGO only suffered minimal changes after the consecutive NIR laser irradiations (Fig. S5E and S5F). Nevertheless, the nanomaterials still retained their nanometric size distribution (Fig. S5E and S5F). Altogether, this data suggests that HA-DOPA-rGO and DOX/HA-DOPA-rGO can be potentially applied in therapeutic regimens involving multiple photothermal effects. These results are also in agreement with the excellent photostability of other graphene-based nanomaterials (Guo et al., 2019; Zhang et al., 2018b).

Finally, the influence of NIR light in the release of DOX from DOX/HA-DOPA-rGO was investigated (Figure S6). In the absence of NIR light, the DOX/HA-DOPA-rGO was able to sustain the release of DOX in a controlled fashion. For instance, only 13, 19, 28 and 38 % of DOX were released from DOX/HA-DOPA-rGO after 3, 6, 24 and 48 h, respectively. Such sustained release is of utmost importance since most nanomedicines display a burst-release of the encapsulated cargoes, which may lead to premature drug leakage during their blood circulation (Maliyakkal et al., 2021; Rodrigues de Azevedo et al., 2017). At the 4 h time mark, the DOX/HA-DOPA-rGO was also irradiated with NIR light (808 nm, 1.7 W/cm^2, 5 min), leading to an improve in the DOX release

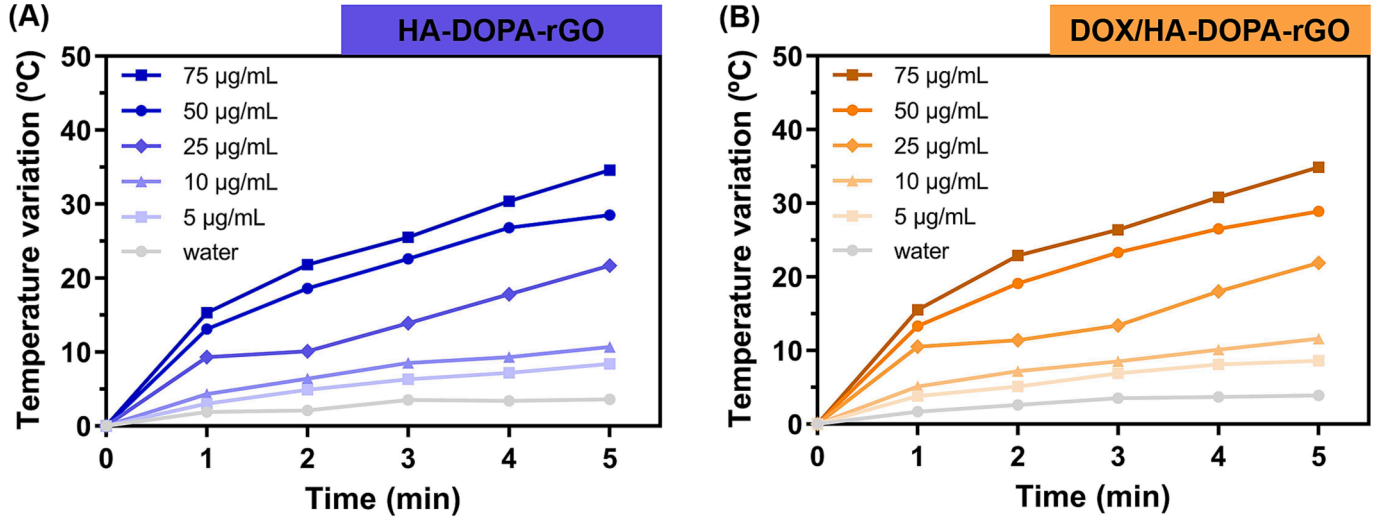

Fig. 2. Temperature variation curves of (A) HA-DOPA-rGO and (B) DOX/HA-DOPA-rGO at different concentrations (of [DOPA-rGO]) throughout 5 min of NIR light irradiation (808 nm, 1.7 W/cm^2).

from 18 to 28 % (Figure S6). In this way, the NIR-light irradiation could enhance the DOX release by up to 1.6-times. After the NIR laser irradiation, the DOX released at 24 and 48 h also rose to 34 and then to 48 %, respectively, further confirming the NIR-responsiveness of DOX/HA-DOPA-rGO.

3.3. Evaluation of the cytocompatibility of HA-DOPA-rGO

Prior to assessing the phototherapeutic capacity of the produced nanomaterials, the cytocompatibility of the HA-DOPA-rGO *per se* (*i.e.*, without its combination with NIR light and DOX) was assessed towards breast cancer (MCF-7) and healthy human (NHDF) cells (Fig. 3).

Both cell lines incubated with the HA-DOPA-rGO nanomaterials, at a wide range of concentrations, did not present any meaningful variations on their viability (Fig. 3). For instance, even at a high dose of 100 μg/mL (of [DOPA-rGO]), and after 24 and 48 h of incubation, the viability of MCF-7 cells was found to be 83 % and 97 %, respectively (Fig. 3A). In turn, NHDF incubated with this same dose of HA-DOPA-rGO for 24 and 48 h displayed a viability of 97 and 80 %, respectively (Fig. 3B). These results are in line with cytocompatible profile of DOPA-rGO nanomaterials and HA-functionalized nanoparticles (Alves et al., 2019; Costa et al., 2023; Lima-Sousa et al., 2021; Vahedi et al., 2022; Xu et al., 2023b).

3.4. Evaluation of HA-DOPA-rGO cellular uptake

Before evaluating the uptake of HA-DOPA-rGO by cells with CD44-receptor overexpression (MCF-7 cells) and without receptor overexpression (NHDF), this nanomaterial was first labelled with RB in order to be analyzed by fluorescence-based techniques (Fig. 4A). The correct labelling was confirmed by assessing the fluorescence emitted by RB/HA-DOPA-rGO (derived from the RB dye). In fact, the RB/HA-DOPA-rGO could emit fluorescence when excited at 514 nm (to be used in CLSM studies; Figure S7B) as well as when excited at 550 nm (to be used in fluorescence spectroscopy assays; Figure S7C). As importantly, the RB/HA-DOPA-rGO also maintained its nanometric size distribution upon the RB labeling (Figure S7A) as well as its surface charge (Figure S4), which is important considering the impact of these features on the nanomaterials' cellular uptake (Augustine et al., 2020).

Initially, the uptake of RB/HA-DOPA-rGO by MCF-7 cells and NHDF was visualized by CLSM. In this regard, RB fluorescence signals were visualized in the cytoplasm of both MCF-7 cells and NHDF after their incubation with RB/HA-DOPA-rGO (Fig. 4C). However, the fluorescence signals were more pronounced in the MCF-7 cells (Fig. 4C and Figure S8). Interestingly, when the MCF-7 cells were pre-treated with free HA prior to their incubation with RB/HA-DOPA-rGO (to saturate the CD44 binding sites), the fluorescence signals in their cytoplasm appeared to decrease to the levels of the NHDF only incubated with the nanomaterials (Fig. 4C). On the other hand, the fluorescence levels on NHDF pre-treated with free HA and incubated with RB/HA-DOPA-rGO were close to those obtained on NHDF only incubated with RB/HA-DOPA-rGO. Taken together, this data advocates for an improved uptake of RB/HA-DOPA-rGO by the CD44-overexpressing MCF-7 cells.

To confirm this hypothesis, the NHDF and MCF-7 cells were also incubated with the RB/HA-DOPA-rGO and, subsequently, were lysed in order to recover the internalized nanomaterials. Then, the RB signals in the cell lysate (corresponding to the internalized RB/HA-DOPA-rGO nanomaterials) were quantified by fluorescence spectroscopy (Fig. 4B). In this regard, the NHDF incubated with RB/HA-DOPA-rGO had a RB fluorescence intensity of 3404 a.u.. In stark contrast, the MCF-7 cells incubated with RB/HA-DOPA-rGO presented a much greater RB fluorescence intensity of 4693 a.u.. In this way, the MCF-7 cells presented 1.4-times higher RB fluorescence signals than NHDF, corroborating an improved uptake of the HA-DOPA-rGO by these breast cancer cells (Fig. 4B). In agreement with CLSM data, the MCF-7 cells pre-treated with free HA and incubated with RB/HA-DOPA-rGO showed a stark decrease in their RB fluorescence signals, being these values (3631 a.u.) very close to those attained on NHDF only exposed to RB/HA-DOPA-rGO (3404 a.u.). As expected, the NHDF pre-treaded with free HA and incubated with RB/HA-DOPA-rGO had an RB fluorescence intensity (3134 a.u.) in line with that of NHDF only incubated with RB/HA-DOPA-rGO (3404 a.u.). These results suggest that the interaction of HA-DOPA-rGO (via its HA-based surface) with the CD44 receptors has a pivotal role in driving the uptake of these nanomaterials by the MCF-7 cells. In fact, other researchers also verified that the functionalization of nanomaterials with HA can also improve their uptake by CD44-overexpressing cells (Gote et al., 2021; Mansoori et al., 2020; Rodrigues et al., 2021). Taken together, this data highlights the ability of HA-DOPA-rGO to be preferentially internalized by the MCF-7 breast cancer cells.

3.5. Evaluation of the photothermal therapy mediated by HA-DOPA-rGO and chemo-photothermal therapy mediated by DOX/HA-DOPA-rGO

After confirming the preferential uptake of HA-DOPA-rGO by the CD44-overexpresisng MCF-7 cells, its phototherapeutic capacity was investigated. For such, this cell line was incubated with HA-DOPA-rGO or DOX/HA-DOPA-rGO, followed by irradiation with NIR light for 5 min (808 nm, 1.7 w/cm^2) (Fig. 5A).

As anticipated, MCF-7 cells incubated with only HA-DOPA-rGO remained highly viable (>96 %), being in agreement with the data reported in the cytocompatibility assays (Fig. 5B and 3A). Moreover, the

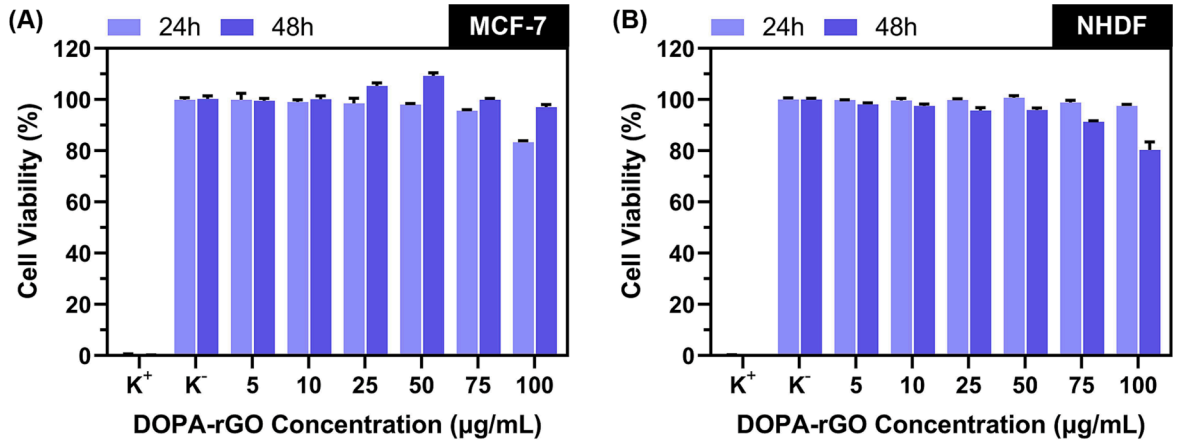

Fig. 3. Cytocompatibility of HA-DOPA-rGO at different concentrations (of [DOPA-rGO]) and incubation times (24 and 48 h) towards (A) MCF-7 cells and (B) NHDF. K^- and K^+ are the negative and positive controls, respectively. Each bar represents the mean ± SD (n = 5).

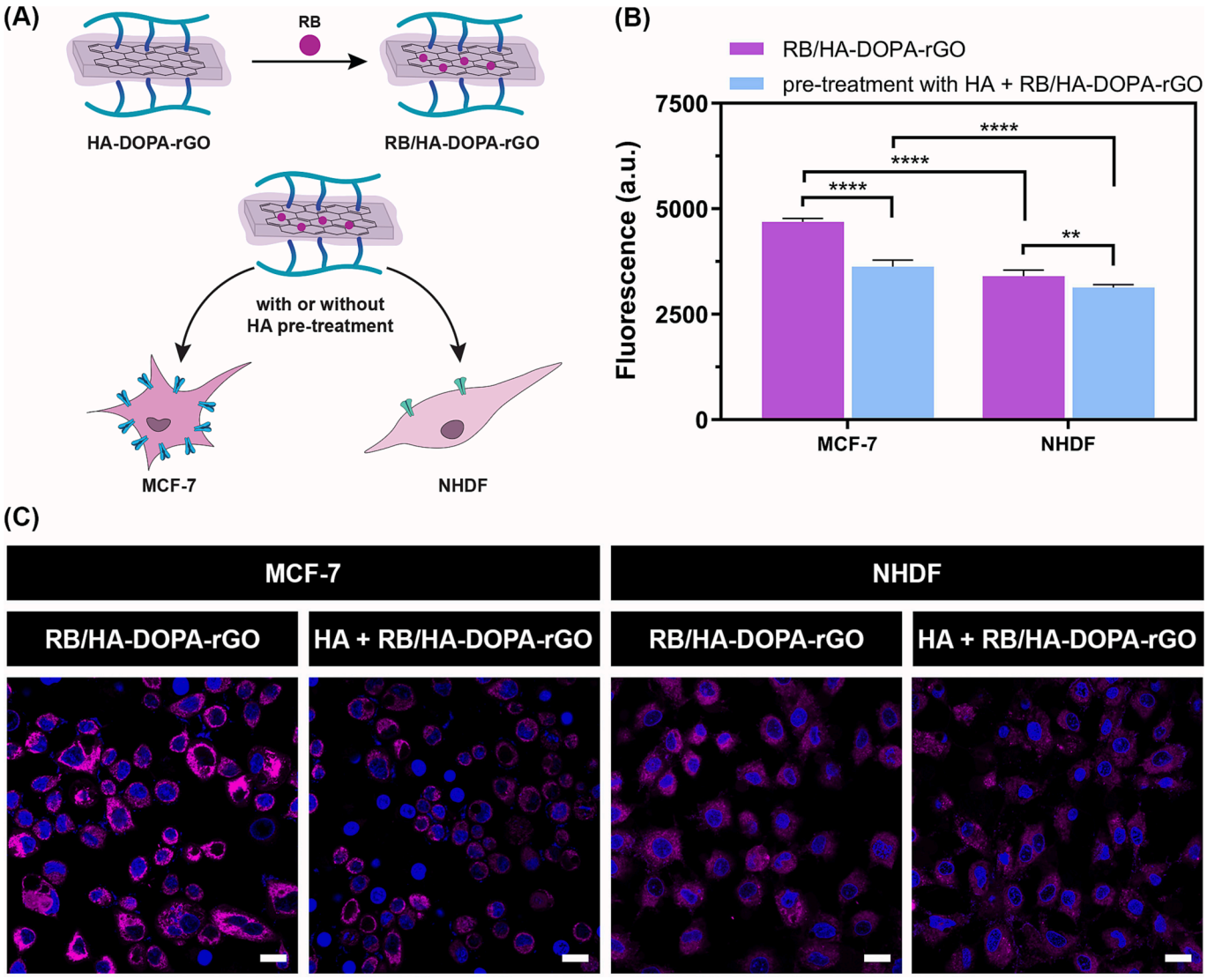

Fig. 4. (A) Schematic illustration of the labelling process of HA-DOPA-rGO with the RB fluorescent dye for investigating its uptake by MCF-7 cells and NHDF. (B) Fluorescent signals of RB/HA-DOPA-rGO (75 μg/mL of [DOPA-rGO]) after 4 h of incubation with MCF-7 cells and NHDF without or with pre-treatment with free HA (HA +). Data represents the mean ± SD (n = 5), $^{**}p < 0.01$, $^{****}p < 0.0001$. (C) Representative CLSM images of the uptake of RB/HA-DOPA-rGO (75 μg/mL of [DOPA-rGO]) by MCF-7 cells and NHDF without or with free HA pre-treatment (HA +). Blue channel: Hoechst 33342® stained nucleus. Pink channel: RB. Scale bars correspond to 20 μm. (For interpretation of the references to colour in this figure legend, the reader is referred to the web version of this article.)

NIR light *per se* did not affect the MCF-7 cells (viability ≈ 99 %; Fig. 5B). This behavior is in-line with the negligible heating induced by the NIR light *per se* (Fig. 2) and with its minimal interactions with biological components (Alves et al., 2022b; Chen et al., 2020; Melo et al., 2021).

On the other hand, the combination of HA-DOPA-rGO (at 75 μg/mL of [DOPA-rGO]) and NIR light was able to reduce the breast cancer cells' viability to about 38 % (nanomaterials' mediated photothermal therapy). In turn, DOX/HA-DOPA-rGO (at 40.5/75 μg/mL of [DOX]/[DOPA-rGO]) was not impactful on breast cancer cells (viability of ≈ 82 %; Fig. 5B). This behavior of the nanomaterials' mediated chemotherapy contrasts with that of the classic chemotherapy (free DOX administration), which decreased the cancer cells viability to about 62 % (Figure S9). In stark contrast, the combination of DOX/HA-DOPA-rGO (at 40.5/75 μg/mL of [DOX]/[DOPA-rGO]) and NIR light was able to diminish the breast cancer cells' viability to just ≈ 23 %. These results were further validated by acquiring CLSM images of the cells stained with calcein-AM (labels live cells) and PI (labels dead cells) exposed to the different treatments (Fig. 6). The enhanced outcome derived from the nanomaterials' mediated chemo-photothermal therapy can be attributed to its multimodal character as well as to the ability of the photoinduced heat to boost the DOX release.

In a work performed by Sun and colleagues, polypyrrole-based nanoparticles (photothermal nanoagent) were coated with a HA-camptothecin conjugate (chemotherapeutic drug), and their combination with NIR light (808 nm, 1.5 W/cm^2, 5 min) could reduce breast cancer cells' viability to about 29 % at the concentration of 500 μg/mL (Sun et al., 2019). In another example, HA-coated nanotube shaped metal–organic frameworks containing DOX and Indocyanine green (photothermal agent), at a dose of 200 μg/mL, could reduce the viability of MDA-MB-231 cells to 31 % upon NIR laser exposure (808 nm, 2.0 W/cm^2, 8 min) (Long et al., 2022). Herein, the combined effect of NIR light (808 nm, 1.7 w/cm^2, 5 min) and DOX/HA-DOPA-rGO reduced the breast cancer cells' viability to just 23 % at a dose of only 40.5/75 μg/mL of [DOX]/[DOPA-rGO].

4. Conclusion

In this work, DOX/HA-DOPA-rGO was prepared as a novel

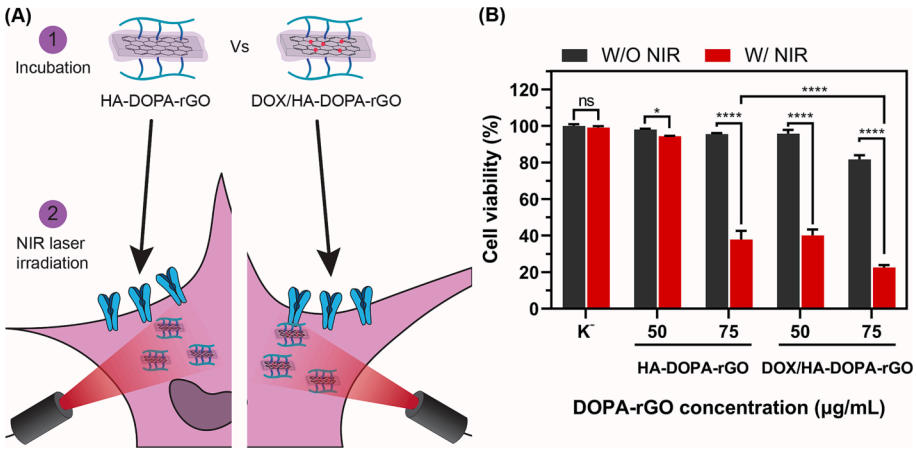

Fig. 5. (A) Schematic representation of the photothermal therapy mediated by HA-DOPA-rGO, and chemo-photothermal therapy mediated by DOX/HA-DOPA-rGO towards MCF-7 cells. (B) Effect of HA-DOPA-rGO (at 50 and 75 μg/mL of [DOPA-rGO]) and DOX/HA-DOPA-rGO (at 27/50 and 40.5/75 μg/mL of [DOX]/[DOPA-rGO]) towards MCF-7 cells without NIR (W/O NIR) and with NIR (W/ NIR) laser irradiation (808 nm, 1.7 W/cm^2, 5 min). K$^-$ W/O NIR represents the negative control and K$^-$ W/ NIR represents cells solely exposed to NIR light. Data represents mean ± SD, n = 5 (*$p < 0.05$; ****$p < 0.0001$), n.s. = non-significant.

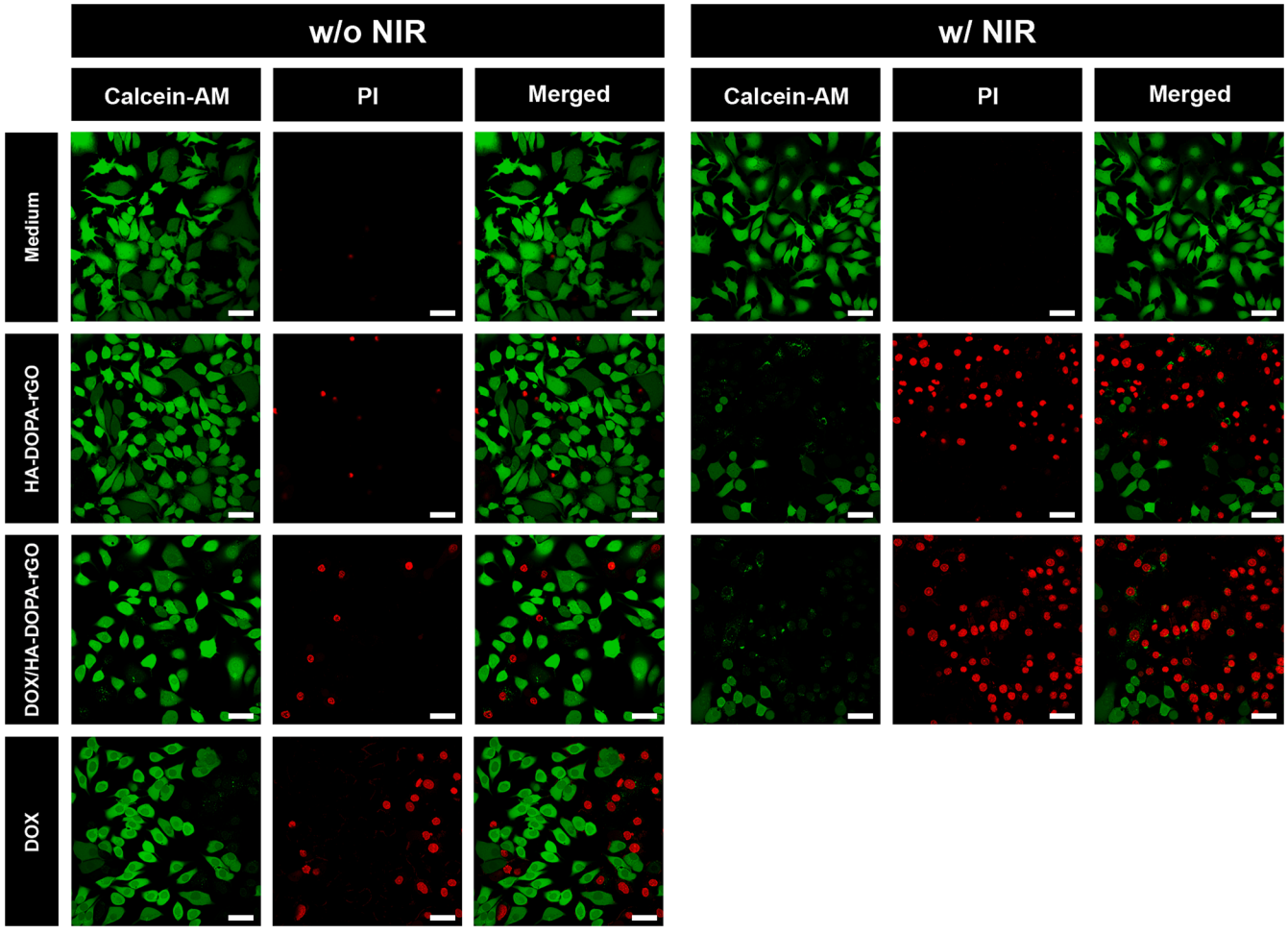

Fig. 6. CLSM images of MCF-7 cells stained with calcein-AM/PI after incubation with HA-DOPA-rGO (at 75 μg/mL of [DOPA-rGO]) or DOX/HA-DOPA-rGO (at 40.5/75 μg/mL of [DOX]/[DOPA-rGO]) W/O NIR or W/ NIR laser irradiation (808 nm, 1.7 W/cm^2, 5 min). Medium W/O NIR and Medium W/ NIR represent the control for live cells and cells only exposed to NIR light, respectively. Green channel: Calcein-AM; red channel: PI. Scale bars correspond to 50 μm. (For interpretation of the references to colour in this figure legend, the reader is referred to the web version of this article.)

covalently functionalized targeted NIR-absorbing nanomaterial for cancer chemo-photothermal therapy. The obtained results revealed that the HA-DOPA-rGO displays a suitable size distribution and surface charge as well as appropriate colloidal stability and cytocompatibility. Moreover, the HA-DOPA-rGO presented an ultra-high and ultra-efficient DOX encapsulation capacity. After irradiation with NIR light, HA-DOPA-

rGO and DOX/HA-DOPA-rGO could produce a temperature increase of about 35 °C. The produced nanomaterials also retained their photothermal capacity after multiple irradiations, displaying an excellent photostability. The findings from the *in vitro* studies showed that the nanomaterials exhibited an enhanced internalization by the CD44-overexpressing MCF-7 cells. In the phototherapeutic studies, the DOX/HA-DOPA-rGO in combination with NIR light decreased the viability of breast cancer cells to just 23 %. Overall, the DOX/HA-DOPA-rGO is a promising nanomaterial for the chemo-photothermal therapy of breast cancer cells. In the future, *in vivo* assays will give an important insight about the safety, tumor-targeting capacity and therapeutic efficacy of this novel multifunctional nanomaterial.

CRediT authorship contribution statement

Rita Lima-Sousa: Conceptualization, Formal analysis, Investigation, Writing – original draft. **Bruna L. Melo:** Investigation, Writing – review & editing. **António G. Mendonça:** Supervision, Writing – review & editing. **Ilídio J. Correia:** Funding acquisition, Project administration, Supervision, Writing – review & editing. **Duarte de Melo-Diogo:** Conceptualization, Funding acquisition, Project administration, Writing – review & editing.

Declaration of competing interest

The authors declare that they have no known competing financial interests or personal relationships that could have appeared to influence the work reported in this paper.

Data availability

Data will be made available on request.

Acknowledgements

This work was developed within the scope of the CICS-UBI projects UIDB/00709/2020 and UIDP/00709/2020, financed by national funds through the Portuguese Foundation for Science and Technology/MCTES. The funding from PTDC/BTABTA/0696/2020, 2022.06320.PTDC (DOI 10.54499/2022.06320.PTDC) and POCI-01-0145-FEDER-022122 is also acknowledged. Duarte de Melo-Diogo acknowledges FCT for the financial support given through a Junior Researcher contract (2021.00590.CEECIND; DOI 10.54499/2021.00590.CEECIND/CP1661/CT0001). Rita Lima-Sousa and Bruna L. Melo acknowledge funding from individual PhD fellowships from FCT (SFRH/BD/144922/2019 and 2021.06044.BD).

Appendix A. Supplementary data

Supplementary data to this article can be found online at https://doi.org/10.1016/j.ijpharm.2023.123763.

References

Alemi, F., Zarezadeh, R., Sadigh, A.R., Hamishehkar, H., Rahimi, M., Majidinia, M., Asemi, Z., Ebrahimi-Kalan, A., Yousefi, B., Rashtchizadeh, N., 2020. Graphene oxide and reduced graphene oxide: Efficient cargo platforms for cancer theranostics. J. Drug Delivery Sci. Technol. 60, 101974 https://doi.org/10.1016/j.jddst.2020.101974.

Alves, C.G., de Melo-Diogo, D., Lima-Sousa, R., Costa, E.C., Correia, I.J., 2019. Hyaluronic acid functionalized nanoparticles loaded with IR780 and DOX for cancer chemo-photothermal therapy. Eur. J. Pharm. Biopharm. 137, 86–94. https://doi.org/10.1016/j.ejpb.2019.02.016.

Alves, C.G., Lima-Sousa, R., Melo, B.L., Ferreira, P., Moreira, A.F., Correia, I.J., Melo-Diogo, D., 2022a. Poly(2-ethyl-2-oxazoline)-IR780 conjugate nanoparticles for breast cancer phototherapy. Nanomedicine (London, U. K.) 17, 2057–2072. https://doi.org/10.2217/nnm-2022-0218.

Alves, C.G., Lima-Sousa, R., Melo, B.L., Moreira, A.F., Correia, I.J., de Melo-Diogo, D., 2022b. Heptamethine cyanine-loaded nanomaterials for cancer immuno-phototherapy/photodynamic therapy: A review. Pharmaceutics 14, 1015. https://doi.org/10.3390/pharmaceutics14051015.

Ankathil, R., 2019. The mechanisms and challenges of cancer chemotherapy resistance: A current overview. Eur. J. Mol. & Clin. Med. 6, 26–34. https://doi.org/10.1007/s10585-018-9903-0.

Ashwinkumar, N., Maya, S., Jayakumar, R., 2014. Redox-responsive cystamine conjugated chitin–hyaluronic acid composite nanogels. RSC Adv. 4, 49547–49555. https://doi.org/10.1039/C4RA06578F.

Attia, M.F., Anton, N., Wallyn, J., Omran, Z., Vandamme, T.F., 2019. An overview of active and passive targeting strategies to improve the nanocarriers efficiency to tumour sites. J. Pharm. Pharmacol 71, 1185–1198. https://doi.org/10.1111/jphp.13098.

Augustine, R., Hasan, A., Primavera, R., Wilson, R.J., Thakor, A.S., Kevadiya, B.D., 2020. Cellular uptake and retention of nanoparticles: Insights on particle properties and interaction with cellular components. Mater. Today Commun. 25, 101692 https://doi.org/10.1016/j.mtcomm.2020.101692.

Blanco, E., Shen, H., Ferrari, M., 2015. Principles of nanoparticle design for overcoming biological barriers to drug delivery. Nat. Biotechnol. 33, 941–951. https://doi.org/10.1038/nbt.3330.

Bukowski, K., Kciuk, M., Kontek, R., 2020. Mechanisms of multidrug resistance in cancer chemotherapy. Int. J. Mol. Sci. 21 https://doi.org/10.3390/ijms21093233.

Chen, G., Cao, Y., Tang, Y., Yang, X., Liu, Y., Huang, D., Zhang, Y., Li, C., Wang, Q., 2020. Advanced near-infrared light for monitoring and modulating the spatiotemporal dynamics of cell functions in living systems. Adv. Sci. (Weinheim, Ger.) 7, 1903783. https://doi.org/10.1002/advs.201903783.

Cheng, Z., Li, M., Dey, R., Chen, Y., 2021. Nanomaterials for cancer therapy: current progress and perspectives. J. Hematol. Oncol. 14, 85. https://doi.org/10.1186/s13045-021-01096-0.

Chien, Y.-H., Chan, K.K., Anderson, T., Kong, K.V., Ng, B.K., Yong, K.-T., 2019. Advanced near-infrared light-responsive nanomaterials as therapeutic platforms for cancer therapy. Adv. Ther. (Weinheim, Ger.) 2, 1800090. https://doi.org/10.1002/adtp.201800090.

Chu, K.F., Dupuy, D.E., 2014. Thermal ablation of tumours: biological mechanisms and advances in therapy. Nat. Rev. Cancer 14, 199–208. https://doi.org/10.1038/nrc3672.

Cintra, E.R., Hayasaki, T.G., Sousa-Junior, A.A., Silva, A.C.G., Valadares, M.C., Bakuzis, A.F., Mendanha, S.A., Lima, E.M., 2022. Folate-targeted PEGylated magnetoliposomes for hyperthermia-mediated controlled release of doxorubicin. Front. Pharmacol. 13 https://doi.org/10.3389/fphar.2022.854430.

Clemons, T.D., Singh, R., Sorolla, A., Chaudhari, N., Hubbard, A., Iyer, K.S., 2018. Distinction between active and passive targeting of nanoparticles dictate their overall therapeutic efficacy. Langmuir 34, 15343–15349. https://doi.org/10.1021/acs.langmuir.8b02946.

Costa, F.J.P., Nave, M., Lima-Sousa, R., Alves, C.G., Melo, B.L., Correia, I.J., de Melo-Diogo, D., 2023. Development of thiol-maleimide hydrogels incorporating graphene-based nanomaterials for cancer chemo-photothermal therapy. Int. J. Pharm. 635, 122713 https://doi.org/10.1016/j.ijpharm.2023.122713.

Domenech, J., Hernández, A., Demir, E., Marcos, R., Cortés, C., 2020. Interactions of graphene oxide and graphene nanoplatelets with the in vitro Caco-2/HT29 model of intestinal barrier. Sci. Rep. 10, 2793. https://doi.org/10.1038/s41598-020-59755-0.

Dutta, B., Barick, K.C., Hassan, P.A., 2021. Recent advances in active targeting of nanomaterials for anticancer drug delivery. Adv. Colloid Interface Sci. 296, 102509 https://doi.org/10.1016/j.cis.2021.102509.

Etter, E.L., Mei, K.C., Nguyen, J., 2021. Delivering more for less: nanosized, minimal-carrier and pharmacoactive drug delivery systems. Adv. Drug Delivery Rev. 179, 113994 https://doi.org/10.1016/j.addr.2021.113994.

Gote, V., Sharma, A.D., Pal, D., 2021. Hyaluronic acid-targeted stimuli-sensitive nanomicelles co-encapsulating paclitaxel and ritonavir to overcome multi-drug resistance in metastatic breast cancer and triple-negative breast cancer cells. Int. J. Mol. Sci. 22, 1257. https://doi.org/10.3390/ijms22031257.

Granja, A., Nunes, C., Sousa, C.T., Reis, S., 2022. Folate receptor-mediated delivery of mitoxantrone-loaded solid lipid nanoparticles to breast cancer cells. Biomed. Pharmacother. 154, 113525 https://doi.org/10.1016/j.biopha.2022.113525.

Guo, D., Yang, H., Zhang, Y., Chen, L., 2019. Constructing mesoporous silica-grown reduced graphene oxide nanoparticles for photothermal-chemotherapy. Microporous Mesoporous Mater. 288, 109608 https://doi.org/10.1016/j.micromeso.2019.109608.

Gyanani, V., Haley, J.C., Goswami, R., 2021. Challenges of current anticancer treatment approaches with focus on liposomal drug delivery systems. Pharmaceuticals 14. https://doi.org/10.3390/ph14090835.

Hernandes, E.P., Lazarin-Bidóia, D., Bini, R.D., Nakamura, C.V., Cótica, L.F., de Oliveira Silva Lautenschlager, S., 2023. Doxorubicin-loaded iron oxide nanoparticles induce oxidative stress and cell cycle arrest in breast cancer cells. Antioxidants (Basel, Switzerland) 12, 237. https://doi.org/10.3390/antiox12020237.

Hua, S., de Matos, M.B.C., Metselaar, J.M., Storm, G., 2018. Current trends and challenges in the clinical translation of nanoparticulate nanomedicines: Pathways for translational development and commercialization. Front. Pharmacol. 9 https://doi.org/10.3389/fphar.2018.00790.

Huang, P., Yang, Y., Wang, W., Li, Z., Gao, N., Chen, H., Zeng, X., 2023. Self-driven nanoprodrug platform with enhanced ferroptosis for synergistic photothermal-IDO immunotherapy. Biomaterials 299, 122157. https://doi.org/10.1016/j.biomaterials.2023.122157.

Huang, N., Zhang, S., Yang, L., Liu, M., Li, H., Zhang, Y., Yao, S., 2015. Multifunctional electrochemical platforms based on the michael addition/schiff base reaction of polydopamine modified reduced graphene oxide: Construction and application. ACS Appl. Mater. Interfaces 7, 17935–17946. https://doi.org/10.1021/acsami.5b04597.

Jiang, Q., Li, X., Yin, C., 2021. A study on improving the efficacy of nanoparticle-based photothermal therapy: From nanoscale to micron scale to millimeter scale. Materials (Basel, Switzerland) 14. https://doi.org/10.3390/ma14092407.

Khafaji, M., Zamani, M., Golizadeh, M., Bavi, O., 2019. Inorganic nanomaterials for chemo/photothermal therapy: A promising horizon on effective cancer treatment. Biophys. Rev. (Heidelberg, Ger.) 11, 335–352. https://doi.org/10.1007/s12551-019-00532-3.

Kim, K., Choi, H., Choi, E.S., Park, M.H., Ryu, J.H., 2019. Hyaluronic acid-coated nanomedicine for targeted cancer therapy. Pharmaceutics 11. https://doi.org/10.3390/pharmaceutics11070301.

Kuderer, N.M., Desai, A., Lustberg, M.B., Lyman, G.H., 2022. Mitigating acute chemotherapy-associated adverse events in patients with cancer. Nat. Rev. Clin. Oncol. 19, 681–697. https://doi.org/10.1038/s41571-022-00685-3.

Li, Z., Chen, Y., Yang, Y., Yu, Y., Zhang, Y., Zhu, D., Yu, X., Ouyang, X., Xie, Z., Zhao, Y., Li, L., 2019. Recent advances in nanomaterials-based chemo-photothermal combination therapy for improving cancer treatment. Front. Bioeng. Biotechnol. 7, 293. https://doi.org/10.3389/fbioe.2019.00293.

Li, Y.-N., Shi, X., Sun, D., Han, S., Zou, Y., Wang, L., Yang, L., Li, Y., Shi, Y., Guo, J., O'Driscoll, C.M., 2023a. Delivery of melarsoprol using folate-targeted PEGylated cyclodextrin-based nanoparticles for hepatocellular carcinoma. Int. J. Pharm. 636, 122791 https://doi.org/10.1016/j.ijpharm.2023.122791.

Li, Z., Yang, L., Zhang, D., Wang, W., Huang, Q., Liu, Q., Shi, K., Yu, Y., Gao, N., Chen, H., Jiang, S., Xie, Z., Zeng, X., 2023b. Mussel-inspired "plug-and-play" hydrogel glue for postoperative tumor recurrence and wound infection inhibition. J. Colloid Interface Sci. 650, 1907–1917. https://doi.org/10.1016/j.jcis.2023.07.154.

Lim, J.H., Choi, H.W., Mo, S.J., Chung, B.G., 2020. Dual-stimuli responsive mesoporous copper (II) sulfide nanocomposite for chemo-photothermal synergistic therapy. Microporous Mesoporous Mater. 302, 110228 https://doi.org/10.1016/j.micromeso.2020.110228.

Lima-Sousa, R., Alves, C.G., Melo, B.L., Moreira, A.F., Mendonça, A.G., Correia, I.J., de Melo-Diogo, D., 2021. Poly(2-ethyl-2-oxazoline) functionalized reduced graphene oxide: Optimization of the reduction process using dopamine and application in cancer photothermal therapy. Mater. Sci. Eng. C 130, 112468 https://doi.org/10.1016/j.msec.2021.112468.

Liu, Y., Zhu, M., Meng, M., Wang, Q., Wang, Y., Lei, Y., Zhang, Y., Weng, L., Chen, X., 2023. A dual-responsive hyaluronic acid nanocomposite hydrogel drug delivery system for overcoming multiple drug resistance. Chinese Chemical Letters 34, 107583. https://doi.org/10.1016/j.cclet.2022.06.006.

Long, Y., Feng, Y., He, Y., Luo, B., Liu, M., 2022. Hyaluronic acid modified halloysite nanotubes decorated with ZIF-8 nanoparticles as dual chemo- and photothermal anticancer agents. ACS Appl. Nano Mater. 5, 5813–5825. https://doi.org/10.1021/acsanm.2c01003.

Maliyakkal, N., Appadath Beeran, A., Udupa, N., 2021. Nanoparticles of cisplatin augment drug accumulations and inhibit multidrug resistance transporters in human glioblastoma cells. Saudi Pharmaceutical Journal 29, 857–873. https://doi.org/10.1016/j.jsps.2021.07.001.

Manivasagan, P., Bharathiraja, S., Santha Moorthy, M., Mondal, S., Nguyen, T.P., Kim, H., Phan, T.T.V., Lee, K.D., Oh, J., 2018. Biocompatible chitosan oligosaccharide modified gold nanorods as highly effective photothermal agents for ablation of breast cancer cells. Polymers 10, 232. https://doi.org/10.3390/polym10030232.

Mansoori, B., Mohammadi, A., Abedi-Gaballu, F., Abbaspour, S., Ghasabi, M., Yekta, R., Shirjang, S.Z., Dehghan, G., Hamblin, M.R., Baradaran, B., 2020. Hyaluronic acid-decorated liposomal nanoparticles for targeted delivery of 5-fluorouracil into HT-29 colorectal cancer cells. J. Cell. Physiol. 235, 6817–6830. https://doi.org/10.1002/jcp.29576.

Melo, B.L., Lima-Sousa, R., Alves, C.G., Ferreira, P., Moreira, A.F., Correia, I.J., de Melo-Diogo, D., 2021. Sulfobetaine methacrylate-albumin-coated graphene oxide incorporating IR780 for enhanced breast cancer phototherapy. Nanomedicine (London, U. K.) 16, 453–464. https://doi.org/10.2217/nnm-2020-0460.

Melo, B.L., Lima-Sousa, R., Alves, C.G., Correia, I.J., de Melo-Diogo, D., 2023. Sulfobetaine methacrylate-coated reduced graphene oxide-IR780 hybrid nanosystems for effective cancer photothermal-photodynamic therapy. Int J Pharm 647, 123552. https://doi.org/10.1016/j.ijpharm.2023.123552.

Mitchell, M.J., Billingsley, M.M., Haley, R.M., Wechsler, M.E., Peppas, N.A., Langer, R., 2021. Engineering precision nanoparticles for drug delivery. Nat. Rev. Drug Discovery 20, 101–124. https://doi.org/10.1038/s41573-020-0090-8.

Nave, M., Costa, F.J.P., Alves, C.G., Lima-Sousa, R., Melo, B.L., Correia, I.J., de Melo-Diogo, D., 2023. Simple preparation of POxylated nanomaterials for cancer chemo-PDT/PTT. Eur. J. Pharm. Biopharm. 184, 7–15. https://doi.org/10.1016/j.ejpb.2023.01.009.

Ortíz, R., Quiñonero, F., García-Pinel, B., Fuel, M., Mesas, C., Cabeza, L., Melguizo, C., Prados, J., 2021. Nanomedicine to overcome multidrug resistance mechanisms in colon and pancreatic cancer: Recent progress. Cancers 13. https://doi.org/10.3390/cancers13092058.

Patel, V., Rajani, C., Tambe, V., Kalyane, D., Anup, N., Deb, P.K., Kalia, K., Tekade, R.K., 2022. Nanomaterials assisted chemo-photothermal therapy for combating cancer drug resistance. J. Drug Delivery Sci. Technol. 70, 103164 https://doi.org/10.1016/j.jddst.2022.103164.

Pearce, A.K., O'Reilly, R.K., 2019. Insights into active targeting of nanoparticles in drug delivery: Advances in clinical studies and design considerations for cancer nanomedicine. Bioconjugate Chem. 30, 2300–2311. https://doi.org/10.1021/acs.bioconjchem.9b00456.

Peltek, O.O., Karpov, T.E., Rogova, A., Postovalova, A., Ageev, E., Petrov, A., Antuganov, D., Stanzhevsky, A.A., Maistrenko, D.N., Zuev, D., Muslimov, A.R., Timin, A.S., Zyuzin, M.V., 2023. Development of nanocarrier-based radionuclide and photothermal therapy in combination with chemotherapy in melanoma cancer treatment. ACS Appl. Mater. Interfaces 15, 13460–13471. https://doi.org/10.1021/acsami.2c20619.

Ren, Y., Yan, Y., Qi, H., 2022. Photothermal conversion and transfer in photothermal therapy: From macroscale to nanoscale. Adv. Colloid Interface Sci. 308, 102753 https://doi.org/10.1016/j.cis.2022.102753.

Robinson, J.T., Tabakman, S.M., Liang, Y., Wang, H., Sanchez Casalongue, H., Vinh, D., Dai, H., 2011. Ultrasmall reduced graphene oxide with high near-infrared absorbance for photothermal therapy. J. Am. Chem. Soc. 133, 6825–6831. https://doi.org/10.1021/ja2010175.

Rodrigues de Azevedo, C., von Stosch, M., Costa, M.S., Ramos, A.M., Cardoso, M.M., Danhier, F., Préat, V., Oliveira, R., 2017. Modeling of the burst release from PLGA micro- and nanoparticles as function of physicochemical parameters and formulation characteristics. Int. J. Pharm. 532, 229–240. https://doi.org/10.1016/j.ijpharm.2017.08.118.

Rodrigues, C.F., Fernandes, N., Melo-Diogo, D.D., Ferreira, P., Correia, I.J., Moreira, A.F., 2021. HA/PEI-coated acridine orange-loaded gold-core silica shell nanorods for cancer-targeted photothermal and chemotherapy. Nanomedicine 16, 2569–2586. https://doi.org/10.2217/nnm-2021-0270.

Schubert, J., Chanana, M., 2018. Coating matters: Review on colloidal stability of nanoparticles with biocompatible coatings in biological media, living cells and organisms. Curr. Med. Chem. 25, 4553–4586. https://doi.org/10.2174/0929867325666180601101859.

Shi, L., Zhang, J., Zhao, M., Tang, S., Cheng, X., Zhang, W., Li, W., Liu, X., Peng, H., Wang, Q., 2021. Effects of polyethylene glycol on the surface of nanoparticles for targeted drug delivery. Nanoscale 13, 10748–10764. https://doi.org/10.1039/D1NR02065J.

Sun, W., Du, Y., Liang, X., Yu, C., Fang, J., Lu, W., Guo, X., Tian, J., Jin, Y., Zheng, J., 2019. Synergistic triple-combination therapy with hyaluronic acid-shelled PPy/CPT nanoparticles results in tumor regression and prevents tumor recurrence and metastasis in 4T1 breast cancer. Biomaterials 217, 119264. https://doi.org/10.1016/j.biomaterials.2019.119264.

Sun, P., Li, Z., Zhang, D., Zeng, W., Zheng, Y., Mei, L., Chen, H., Gao, N., Zeng, X., 2024. Multifunctional biodegradable nanoplatform based on oxaliplatin prodrug cross-linked mesoporous polydopamine for enhancing cancer synergetic therapy. Chinese Chemical Letters 35, 108346. https://doi.org/10.1016/j.cclet.2023.108346.

Tian, H., Zhang, T., Qin, S., Huang, Z., Zhou, L., Shi, J., Nice, E.C., Xie, N., Huang, C., Shen, Z., 2022. Enhancing the therapeutic efficacy of nanoparticles for cancer treatment using versatile targeted strategies. J. Hematol. Oncol. 15, 132. https://doi.org/10.1186/s13045-022-01320-5.

Vahedi, N., Tabandeh, F., Mahmoudifard, M., 2022. Hyaluronic acid–graphene quantum dot nanocomposite: Potential target drug delivery and cancer cell imaging. Biotechnol. Appl. Biochem. 69, 1068–1079. https://doi.org/10.1002/bab.2178.

Wang, F., Li, J., Chen, C., Qi, H., Huang, K., Hu, S., 2022. Preparation and synergistic chemo-photothermal therapy of redox-responsive carboxymethyl cellulose/chitosan complex nanoparticles. Carbohydr. Polym. 275, 118714 https://doi.org/10.1016/j.carbpol.2021.118714.

Wei, G., Wang, Y., Yang, G., Wang, Y., Ju, R., 2021. Recent progress in nanomedicine for enhanced cancer chemotherapy. Theranostics 11, 6370–6392. https://doi.org/10.7150/thno.57828.

Xu, X.J., Li, Y., Hui, H., Liu, C.L., Fu, Y., Yang, H.Y., 2023b. Dual-targeting multifunctional hyaluronic acid ligand-capped gold nanorods with enhanced endo-lysosomal escape ability for synergetic photodynamic–photothermal therapy of cancer. Biotechnol. Bioeng. 1–12 https://doi.org/10.1002/bit.28462.

Xu, J., Song, M., Fang, Z., Zheng, L., Huang, X., Liu, K., 2023a. Applications and challenges of ultra-small particle size nanoparticles in tumor therapy. J. Controlled Release 353, 699–712. https://doi.org/10.1016/j.jconrel.2022.12.028.

Yan, W., Leung, S.S.Y., To, K.K.W., 2020b. Updates on the use of liposomes for active tumor targeting in cancer therapy. Nanomedicine (London, U.K.) 15, 303–318. https://doi.org/10.2217/nnm-2019-0308.

Yan, L., Shen, J., Wang, J., Yang, X., Dong, S., Lu, S., 2020a. Nanoparticle-Based Drug Delivery System: A Patient-Friendly Chemotherapy for Oncology. Dose Response 18, 1559325820936161. https://doi.org/10.1177/1559325820936161.

Yao, Y., Zhou, Y., Liu, L., Xu, Y., Chen, Q., Wang, Y., Wu, S., Deng, Y., Zhang, J., Shao, A., 2020. Nanoparticle-based drug delivery in cancer therapy and its role in overcoming drug resistance. Frontiers in Molecular Biosciences 7, 193. https://doi.org/10.3389/fmolb.2020.00193.

Zhang, W., Dai, J., Zhang, G., Zhang, Y., Li, S., Nie, D., 2018b. Photothermal/pH dual-responsive drug delivery system of amino-terminated HBP-modified rGO and the chemo-photothermal therapy on tumor cells. Nanoscale Research Letters 13, 379. https://doi.org/10.1186/s11671-018-2787-8.

Zhang, X., Wang, S., Cheng, G., Yu, P., Chang, J., 2022a. Light-responsive nanomaterials for cancer therapy. Engineering 13, 18–30. https://doi.org/10.1016/j.eng.2021.07.023.

Zhang, L., Xia, J., Zhao, Q., Liu, L., Zhang, Z., 2010. Functional graphene oxide as a nanocarrier for controlled loading and targeted delivery of mixed anticancer drugs. Small 6, 537–544. https://doi.org/10.1002/smll.200901680.

Zhang, X., Yan, R., Wei, Z., Yang, D., Hu, Z., Zhang, Y., Huang, X., Huang, H., Wang, W., 2022b. Folate decorated multifunctional biodegradable nanoparticles for gastric

carcinoma active targeting theranostics. Int. J. Nanomed. 17, 2493–2502. https://doi.org/10.2147/IJN.S348380.

Zhang, S., Zhang, D., Li, Z., Yang, Y., Sun, M., Kong, Z., Wang, Y., Bai, H., Dong, W., 2018a. Polydopamine functional reduced graphene oxide for enhanced mechanical and electrical properties of waterborne polyurethane nanocomposites. J. Coat. Technol. Res. 15, 1333–1341. https://doi.org/10.1007/s11998-018-0082-3.

Zhong, L., Li, Y., Xiong, L., Wang, W., Wu, M., Yuan, T., Yang, W., Tian, C., Miao, Z., Wang, T., Yang, S., 2021. Small molecules in targeted cancer therapy: advances, challenges, and future perspectives. Signal Transduction Targeted Ther. 6, 201. https://doi.org/10.1038/s41392-021-00572-w.